energies

MDPI

Article

Clarifications on the Behavior of Alternative Gases to SF_6 in Divergent Electric Field Distributions under AC Voltage

Houssem Eddine Nechmi [1,*], Michail Michelarakis [1], Abderrahmane (Manu) Haddad [1] and Gordon Wilson [2]

[1] Advanced High Voltage Engineering Research Centre, School of Engineering, Cardiff University, The Parade, Cardiff CF24 3AA, UK; michelarakism@cardiff.ac.uk (M.M.); haddad@cardiff.ac.uk (A.H.)
[2] National Grid House, (Floor C3), Warwick Technology Park, Gallows Hill, Warwick CV34 6DA, UK; gordon.wilson@nationalgrid.com
* Correspondence: NechmiH@cardiff.ac.uk; Tel.: +44-29208-76390

Abstract: Negative and positive partial discharge inception voltages and breakdown measurements are reported in a needle-plane electrode system as a function of pressure under AC voltage for natural gases (N_2, CO_2, and O_2/CO_2), pure Novec^{TM} gases (C_4F_7N and $C_5F_{10}O$) and Novec^{TM} in different natural gas admixtures. For compressed 4% C_4F_7N–96% CO_2 and 6% $C_5F_{10}O$–12% O_2–82% CO_2 gas mixtures, the positive-streamer mode is identified as the breakdown mechanism. Breakdown and negative partial discharge inception voltages of 6% $C_5F_{10}O$–12% O_2–82% CO_2 are higher than those of 4% C_4F_7N–96% CO_2. At 8.8 bar abs, the breakdown voltage of 6% $C_5F_{10}O$–12% O_2–82% CO_2 is equal to that of 12.77% O_2–87.23% CO_2 (buffer gas). Synergism in negative partial discharge inception voltage/electric field fits with the mean value and the sum of each partial pressure individually component for a 20% C_4F_7N–80% CO_2 and 6% $C_5F_{10}O$–12% O_2–82% CO_2, respectively. In 9% C_4F_7N–91% CO_2, the comparison of partial discharge inception electric fields is E_{max} (CO_2) = E_{max}(C_4F_7N), and E_{max} (12.77% O_2–87.23% CO_2) = E_{max}($C_5F_{10}O$) in 19% $C_5F_{10}O$–81%(12.77% O_2–87.23% CO_2). Polarity reversal occurs under AC voltage when the breakdown polarity changes from negative to positive cycle. Polarity reversal electric field E_{PR} was quantified. Fitting results show that E_{PR} (CO_2) = E_{PR}(9% C_4F_7N–91% CO_2) and E_{PR}(SF_6) = E_{PR} (22% C_4F_7N–78% CO_2). E_{PR} (4% C_4F_7N–96% CO_2) = E_{PR} (12.77% O_2–87.23% CO_2) and E_{PR} (6% $C_5F_{10}O$–12% O_2–82% CO_2) < E_{PR} (4% C_4F_7N–96% CO_2) < E_{PR} (CO_2).

Keywords: N_2; O_2/CO_2; C_4F_7N; C_4F_7N/CO_2; $C_5F_{10}O$; $C_5F_{10}O/O_2/CO_2$; gaseous breakdown; divergent electric fields; partial discharge inception voltage/electric field; polarity reversal pressure/electric field

Citation: Nechmi, H.E.; Michelarakis, M.; (Manu) Haddad, A.; Wilson, G. Clarifications on the Behavior of Alternative Gases to SF_6 in Divergent Electric Field Distributions under AC Voltage. *Energies* **2021**, *14*, 1065. https://doi.org/10.3390/en14041065

Academic Editor: Anna Rita Di Fazio

Received: 19 January 2021
Accepted: 16 February 2021
Published: 18 February 2021

1. Introduction

In compressed SF_6 [1–5], the propagation mechanism (leader criterion) is the breakdown mode in the presence of conducting particles fixed/floating on conductors or insulators. In the presence of invasive pollutants, the streamer inception level is lower than the leader inception level. The conventional partial discharge (PDs) measurement technique constitutes a means to detect the presence of defects without conducting destructive tests.

On the other hand, for C_4F_7N/CO_2 mixtures [6], the PDs activity under AC voltage varies as a function of pressure and the magnitude of the electric field, including breakdown polarity reversal (PR), when the AC breakdown polarity changes from negative half-cycle to positive half-cycle with the increase of pressure. At the reversal critical pressure (PR pressure), breakdowns occur on positive or negative half-cycles. Before PR, PDs are observed during the negative half-cycle, and current pulses occur on the positive cycle. For the same electric field distribution, increasing the pressure leads to an increase of the partial discharge inception voltage (PDIV) and an increase of the intensity of the maximum electric field on the tip of the needle. The latter causes inception of a denser PDs activity on the positive cycle and an attenuation of the PDs on the negative cycle. For pressures above PR,

negative PDs activity decreases until being hidden by the background noise of the current sensing circuit. In this case, only higher positive polarity PDs activity is detectable, and the positive PDIV is close to breakdown. It was reported that the breakdown voltage is equal under positive and negative polarities under lightning impulse voltage waveform in quasi-uniform fields and at PR pressure [7,8]. The PR pressure increases linearly with the increase of field utilization factor η given by Equation (1). It should be noted that $\eta = E_{mean}/E_{max}$, E_{max} being the maximum electric field for a given electrode configuration; it is computed using finite element method simulation using COMSOL Multiphysics^{TM} software.; and E_{mean} is the mean electric field given by $E_{mean} = V/d$ where V is the applied voltage and d is the electrodes gap. The linear increase is characterized by a constant polarity reversal electric field E_{PR} calculated according to Equation (1), where V_i is the positive PDIV for divergent electric fields and the breakdown voltage for quasi-uniform electric fields, d is the electrode gap. Table 1 reports E_{PR} for different gas/gas mixtures [6–8].

$$(E_{PR} \text{ or } E_{max}) = \frac{V_i}{d \cdot n} \quad (1)$$

Table 1. Reported polarity reversal electric field E_{PR} according to Equation (1) [6–8].

Gas/Gas Mixture	E_{PR} (kV/mm)	Pressure (bar abs)	η
SF_6 [7,8]	86	7.5	0.17
CO_2 [6]	64	2.5	0.0385
3.7% C_4F_7N–96.3% CO_2 [8]	47	9.5	0.33
10% C_4F_7N–90% CO_2 [7]	66	5.5	0.22

The present work investigates both the negative/positive-inception and breakdown voltages of a classic defect in GIS (fixed particle on the live conductor) under AC voltage waveform for different gases and gas mixtures. Natural gases, such as N_2, CO_2, and O_2/CO_2, are also assessed since they constitute the buffer gas(es) when mixed with the fluorinated SF_6 replacement candidates (C_4F_7N or $C_5F_{10}O$). The main purpose of adding natural gases is to lower the boiling point of the final fluorinated/natural gas mixture to reach operating temperatures similar to SF_6 for indoor and outdoor high voltage applications. In addition, pure C_4F_7N and $C_5F_{10}O$ were studied at the sub-atmospheric pressure level without liquefaction. Then, including minimal working temperature and its corresponding concentrations [7–9], the addition of highly electronegative gases to natural gases is investigated, and the synergism of the constituents is quantified. Inception electric field was calculated in positive/negative polarities for pure/gas mixtures, and synergism laws are deducted. The polarity reversal electric fields are calculated for the C_4F_7N/CO_2 and $C_5F_{10}O/O_2/CO_2$ gas mixtures.

2. Materials and Methods

To study pure gas/gas mixture pre-breakdown and breakdown characteristics under non-uniform fields, a needle/plane defect model was utilized as described in previous work [6]. The needle was placed between two plane electrodes of Bruce profile to provide homogeneous background electric field conditions. The plane electrodes were made of aluminum and the 100 μm tip radius needle from tungsten of 99.99% purity. The electrode set was placed inside a vessel made of stainless steel (volume = 12 L, max pressure = 12 bar abs). The high voltage needle electrode that was connected to the bushing was fixed and was connected to a high voltage AC source (3.75 kVA) with a maximum output voltage of 50 kV rms. The high voltage bushing installed on the test vessel was rated at 38 kV AC rms. The grounded plane electrode, however, was vertically moveable within the test chamber so that the desired gap length can be achieved with an accuracy of 0.1 mm. Current sensing was performed by coupling a high-frequency current transformer (HFCT), of 500 MHz

upper cutoff frequency, to the lower (grounded) plane electrode, while the recording of the generated signals was performed through a 500 MHz, 2 GS/s oscilloscope (see Figure 1).

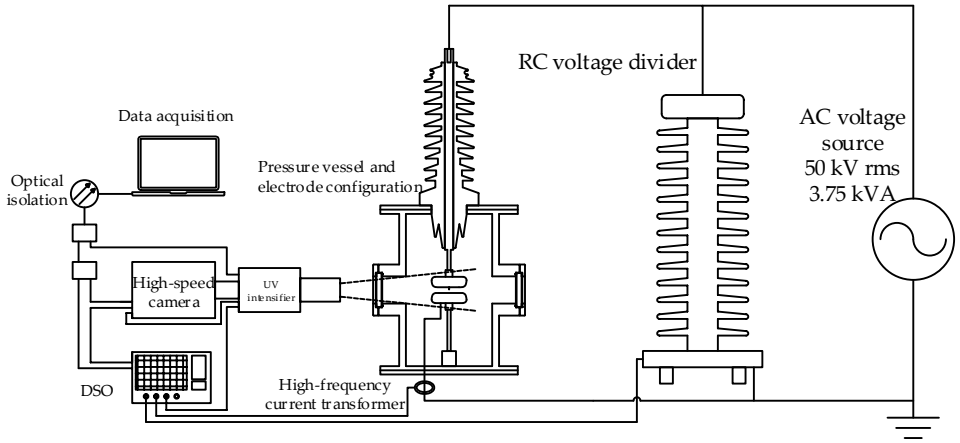

Figure 1. Experimental circuit.

Figure 2 shows the field utilization factor η given by Equation (1) of the experimental arrangement as a function of gap distance. Such an electrode configuration gives a constant field utilization factor η = 0.0385 for gaps between 10 mm and 20 mm. For a 60 kV peak AC applied voltage, η = 0.0385 and d = 10 mm, the maximum electric field E_{max} is ≈156 kV/mm.

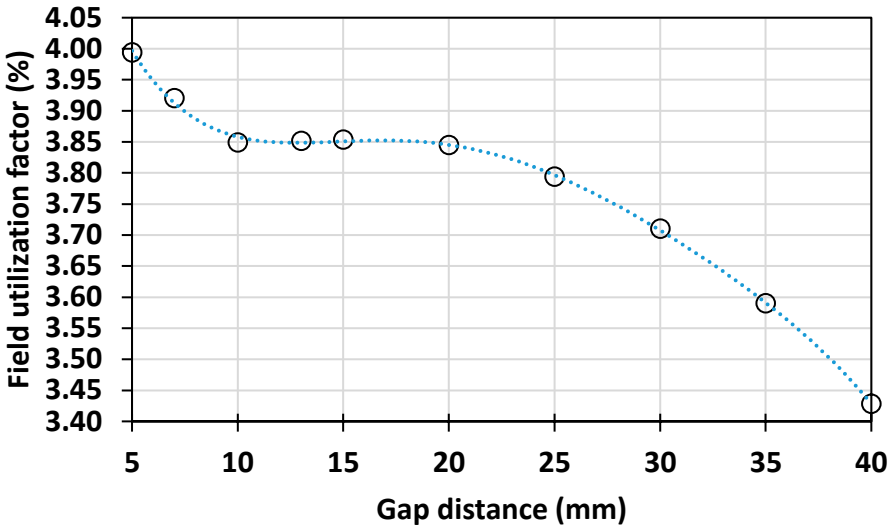

Figure 2. Calculated field utilization factor η at various gap distances.

The different investigated gas/gas mixtures are listed in Table 2. A Dilo (mini-series ^{C5} and mini-series ^{C4}) was used to circulate the Novec^{TM} 5110 ($C_5F_{10}O$) and Novec^{TM} 4710 (C_4F_7N) mixtures in the gaseous state. For a 6% $C_5F_{10}O$/12% O_2/82% CO_2 gas mixture [9], a premixed 12.77% O_2/87.23% CO_2 gas mixture was used for the preparation of the gas mixture and representing the buffer gas.

The inception voltage of pre-breakdown discharges, which originated from the needle tip, was investigated optically in the visible and ultraviolet light emission spectrum. The optical detection system consisted of a UV image intensifier, incorporating an S20 photocathode, mounted on the front of an 8-bit high-speed camera with a maximum resolution of 1024 × 1024 px. A chromatically corrected Nikon UV-105, 105 mm f/4.5 lens was installed on the optical input of the intensifier. Observations were performed through a UV-grade fused silica side viewport installed on the pressure vessel. The entire camera system was

aligned to and focus adjusted towards the installed electrode configuration. A UV band-pass filter mounted on the front of the UV lens was used to absorb the visible spectrum light emitted by glow discharge. While current detection was difficult and sometimes impossible in the high-pressure range (at pressure levels between 5 and 10 bar abs), using a high-frequency current transformer (500 MHz) of high gain ratio (5 V/A), combined with the camera system described above, consisted an effective method to detect PDIV in the UV and VIS spectral range. Figure 3 shows an example of a negative-streamer light emission image of N_2 at 5 bar abs.

Table 2. List of investigated gases and gas mixtures.

Gas/Gas Mixture	Maximum Pressure (bar abs)
CO_2	8.8
N_2	8.8
12.77% O_2–87.23% CO_2	10
$C_5F_{10}O$	0.6
6% $C_5F_{10}O$–12% O_2–82% CO_2	10
C_4F_7N	1
4% C_4F_7N–96% CO_2	10
20% C_4F_7N–80% CO_2	5

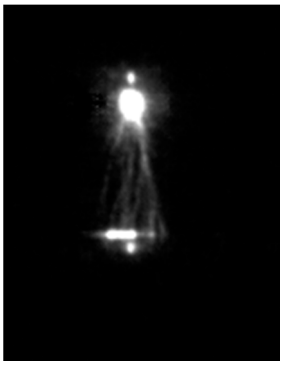

Figure 3. Negative-streamer propagation in N_2 (d = 10 mm, 5 bar abs).

A new needle was used for each gas/gas mixture to prevent deformation in the radius of the needle and biased results. No erosion effect on needle tips was observed after partial discharge inception voltage (PDIV) measurements. Initially, the PDIV was investigated, followed by breakdown voltage (BDV) measurements. No difference in BDV results was observable between new and used needles up to a certain limit; however, the needle was replaced frequently (see Figure 4). In contrast, one single BDV caused a decrease in PDIV.

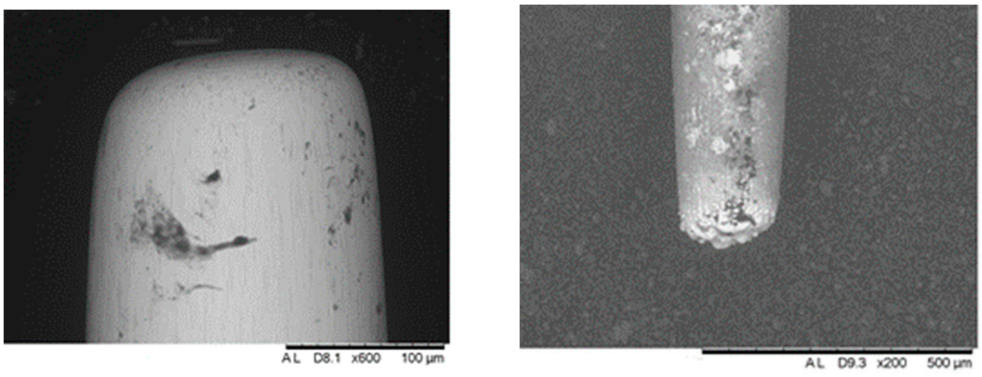

(**a**) (**b**)

Figure 4. Scanning electron microscope image of 100 µm radius needle: (**a**) no breakdown, non-arced (×600) and (**b**) after several breakdowns, arced (×200).

For breakdown measurements, an AC voltage ramp was increased at a rate of 2 kV/s up to 90% of the voltage level that initiated electrical discharges, and then 0.1 kV/s was used. For each breakdown event, measurement series of 10 individual discharges were performed. Three minutes were kept in between the individual electrical discharges. The test rig bushing flashover limit was 60 kV peak. The ramp method was employed to identify the inception voltage of partial discharge. The voltage was increased with the rate of 1 kV/s until the first pulse, or a light emission image (UV-vis spectrum), was detected.

3. Results

3.1. Natural Gases

N_2, CO_2, O_2/CO_2 mixtures are interesting because they are perfectly ecologically compatible, and they constitute a major part of the atmosphere. The pure nitrogen used contains around 0.01% oxygen. Here, negative and positive-inception voltages and AC breakdown measurements are reported for N_2 at various pressures up to 8.8 bar abs (see Figure 5). The effect of needle condition (non-arced vs. arced) was investigated. After breakdown measurements (arced needle), a change in negative-inception voltage was observed at high pressure, and a saturation trend occurs. To prevent this deviation, inception voltage was measured first, followed by breakdowns for all the following measurements. For each gas/gas mixture, a new needle was used. The negative-inception voltage increases linearly as the gas pressure increases. An example of negative-inception voltage–current characteristics and its visual proof (UV vs. UV + VIS) at 8.8 bar abs is shown in Figure 6. The captures show that it contained combined ultraviolet and visible emitted light. The glow discharge is detectable across the pressure range (see Figure 7).

Figure 5 shows a deviation between breakdown and negative-inception voltages at 5 bar abs, corresponding to an electric field of 67 mkV/mm according to Equation (1). By increasing the pressure, deviation increased. Positive-current pulses were detectable for pressures above 6 bar abs (see Figures 5 and 8).

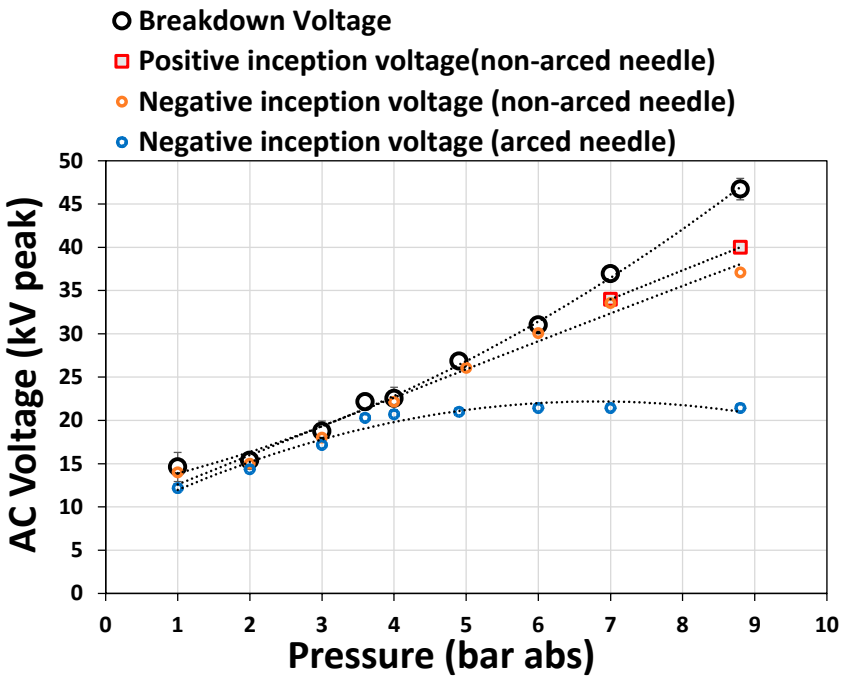

Figure 5. V_{mean} breakdown, positive and negative-inception voltages as a function of gas pressure (N_2, d = 10 mm).

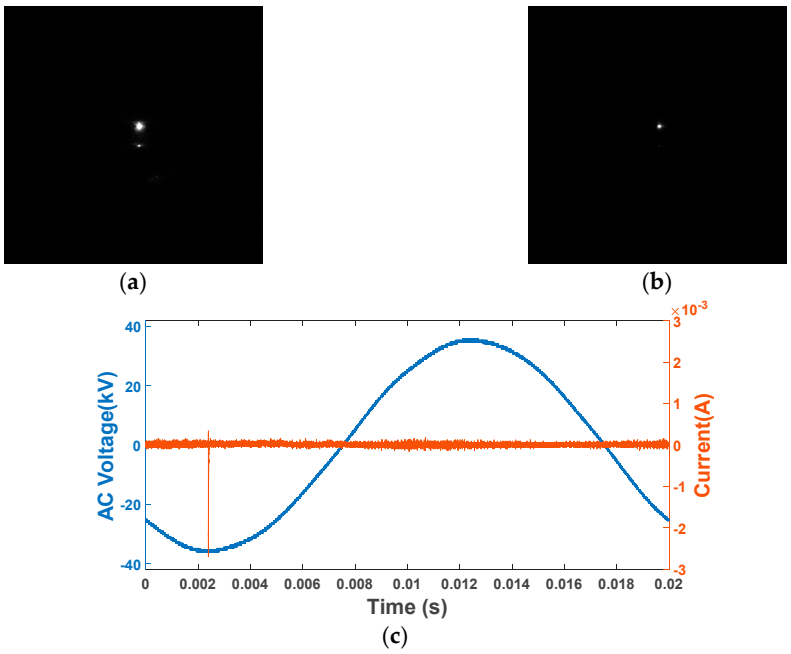

Figure 6. Negative-inception voltage in N_2: d = 10 mm, p = 8.8 bar abs, V = 37 kV, G_I = 60% is the relative luminous gain of the recording system in the: (**a**) visible + ultraviolet light (UV + VIS) (**b**) ultraviolet radiation emission images (UV) and (**c**) associated voltage–current waveform (negative-inception voltage).

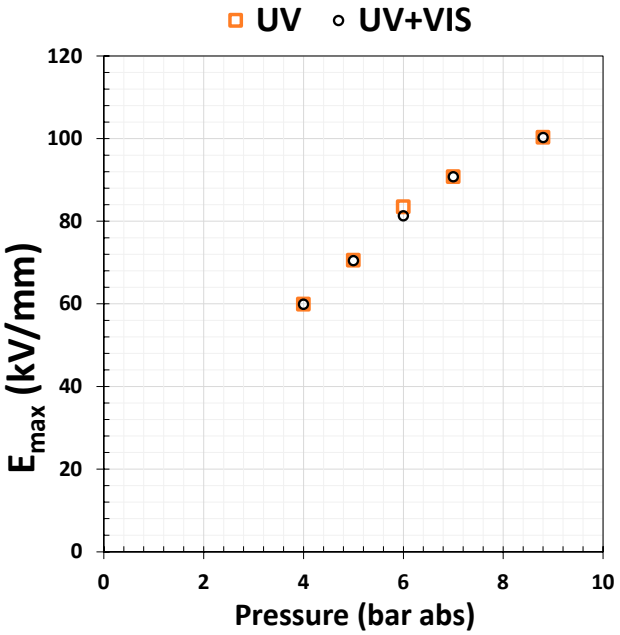

Figure 7. Negative-inception electric field in the visible +ultraviolet light and ultraviolet radiation along the electromagnetic spectrum, as a function of gas pressure (N_2, d = 10 mm, G_I = 60% is the relative luminous gain of the image recording system).

The breakdown voltage of N_2 showed a linear dependence on increasing gas pressure in contrast to electronegative gas/gas mixtures that present nonlinear tendency for the same needle-plane configuration, such as CO_2 and 4% C_4F_7N–96% CO_2 [6]. The breakdown occurred exclusively under a negative AC voltage peak for the pressure range. According to the pre-breakdown current measurements (see Figure 8) and the optical observations

(see Figures 3 and 8), the negative glow streamer mode was identified as the breakdown mechanism for compressed N_2. These findings agree with previous investigations [10–15].

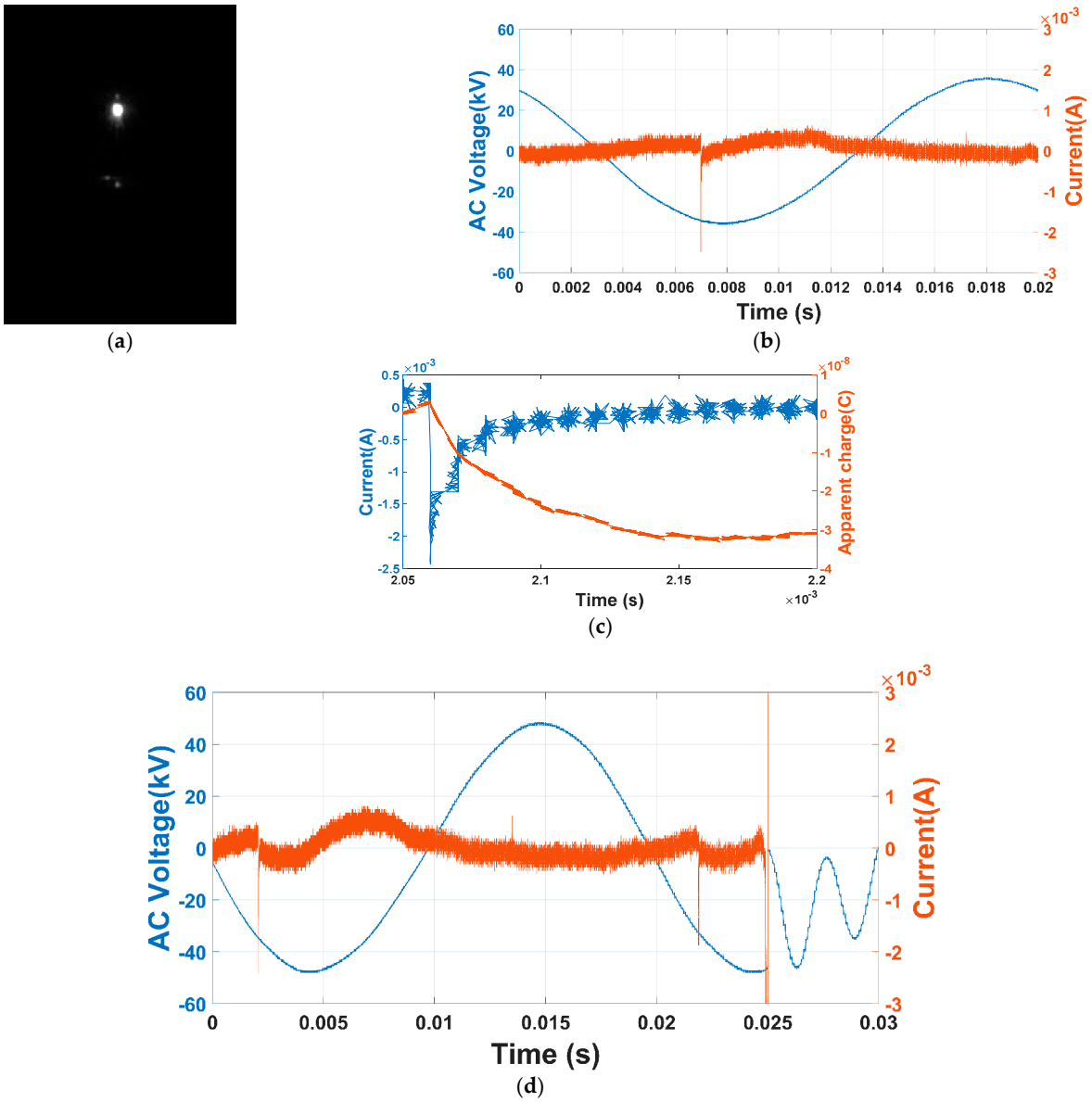

Figure 8. Voltage–current waveform for measuring (**a**) partial discharge, on negative-streamer emission image (VIS + UV), (**b**) associated current, (**c**) apparent charge and (**d**) breakdown voltages, on the negative half-cycle (N_2, d = 10 mm p = 8.8 bar abs).

Figure 9 summarizes the negative and the positive-inception voltage and AC breakdown measurement for 12.77% O_2–87.23% CO_2 at various pressures up to 10 bar abs. The negative-inception voltage increased linearly with the increase of gas pressure. An example of negative and positive partial discharge voltage–current characteristics and its emission image (UV + VIS) at 8.8 bar abs are shown in Figure 10. The intensity of negative partial discharge current decreased with an increase of pressure (see Figure 11a). The breakdown characteristic of 12.77% O_2–87.23% CO_2 showed a nonlinear behavior when the gas pressure increased. The breakdown occurred under the negative AC voltage peak for pressures below 1.6 bar abs and on the positive AC voltage peak above. The polarity reversal (PR) cross point at 1.6 bar abs corresponds to a positive-inception electric field of 50 kV/mm, calculated according to Equation (1). At pressures below PR, only negative

PDs were detectable up to breakdown. At PR pressure, similar partial discharge activities occurred on positive and negative cycles (see Figure 10a). The luminosity of the positive cycle was lower than that of the negative cycle (see Figure 10b,c). At pressures above PR [3,6], the needle tip was covered with a cloud of charge carriers, which were stabilized by negative ions formed by the attachment of electrons. Consequently, the negative space charges generate a reduction of the electric field on the side of the tip. This causes an increase in the breakdown voltage. For high pressure (8.8 bar abs), one positive-current pulse was detectable before the breakdown; the positive-streamer channels transited to leader channels and arrived at the opposite electrode instantly. The space charge near the needle tip resulted in a reduced electric field. The electrode was virtually elongated, the gap width was reduced, and the electric field was enhanced in the remaining gap, resulting in a reduction in breakdown voltage. It established an electrical conduction path between the two electrodes. Heating and expansion of the conductive channel occurred, and multiple branches were created (see Figure 11c). The negative partial discharge inception voltage (PDIV) was identified with current and emission light images. The negative partial discharge inception electric field (PDIEF) E_{max} was calculated according to Equation (1) for different natural gases as a function of pressure. The results are shown in Figure 12. Along the pressure range investigated, PDIEF of N_2 and 12.77% O_2–87.23% CO_2 exhibits a linear trend. On the other hand, PDIEF of CO_2 evolved linearly and presented a saturation trend at higher pressure levels (>5 abs). As a result, at the highest and lowest pressures (8.8 bar abs and 1 bar abs), PDIEF (12.77% O_2–87.23% CO_2) > PDIEF (CO_2) > PDIEF (N_2). However, at the intermediate pressures, PDIEF (CO_2) was higher than PDIEF (12.77% O_2–87.23% CO_2 and N_2) and PDIEF (N_2) = PDIEF (12.77% O_2–87.23% CO_2).

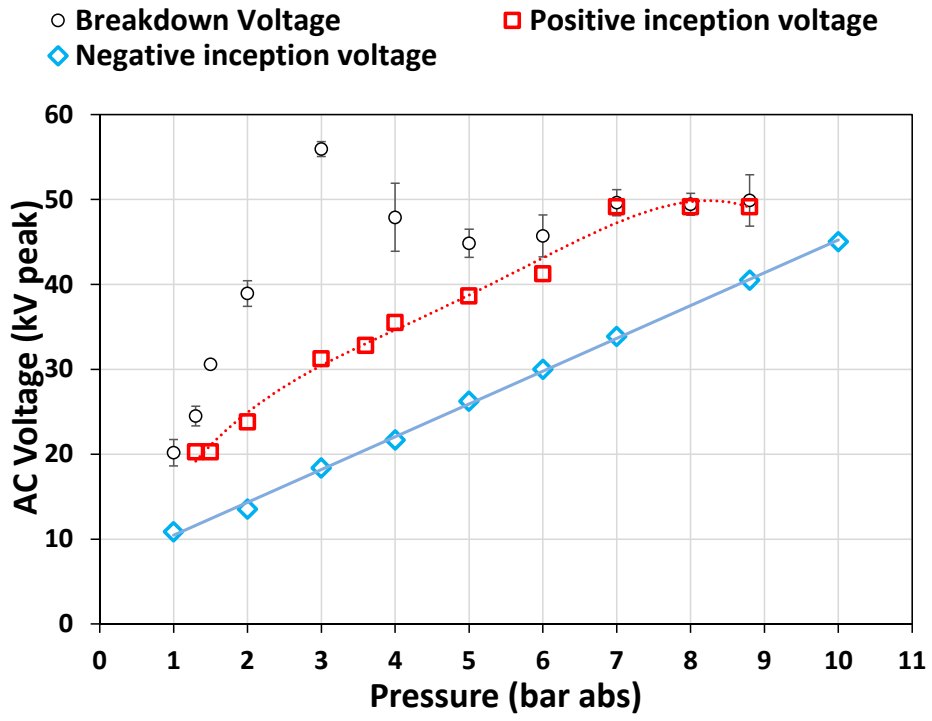

Figure 9. V_{mean} breakdown, positive and negative-inception voltages as a function of gas pressure (12.77% O_2–87.23% CO_2, d = 10 mm).

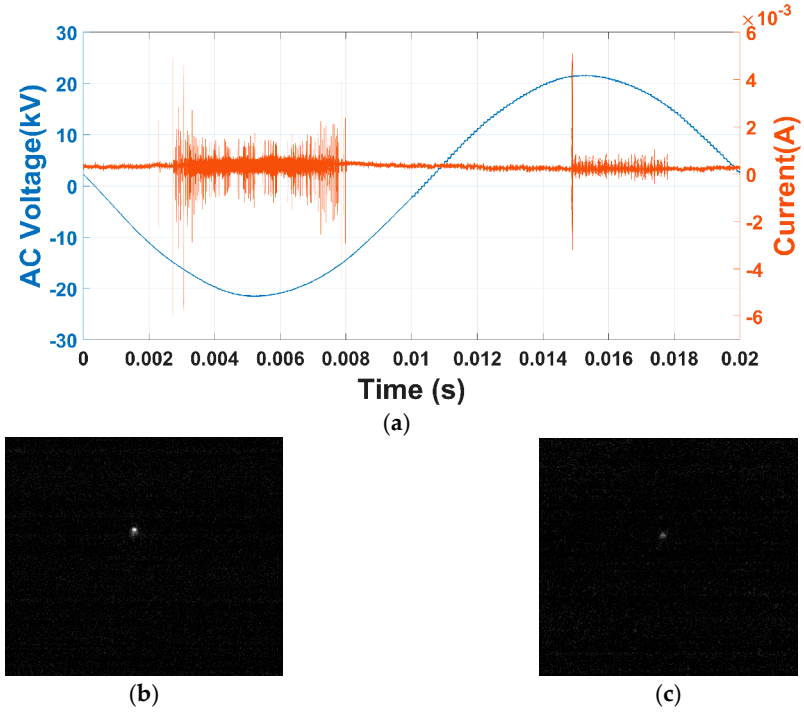

Figure 10. Voltage–current waveform for measuring (**a**) partial discharge at polarity reversal (PR) pressure in 12.77% O_2–87.23% CO_2 (d = 10 mm, P = 1.6 bar abs). G_I = 60% is the relative luminous gain of the recording system in the VIS + UV range for (**b**) negative cycle and (**c**) positive cycle.

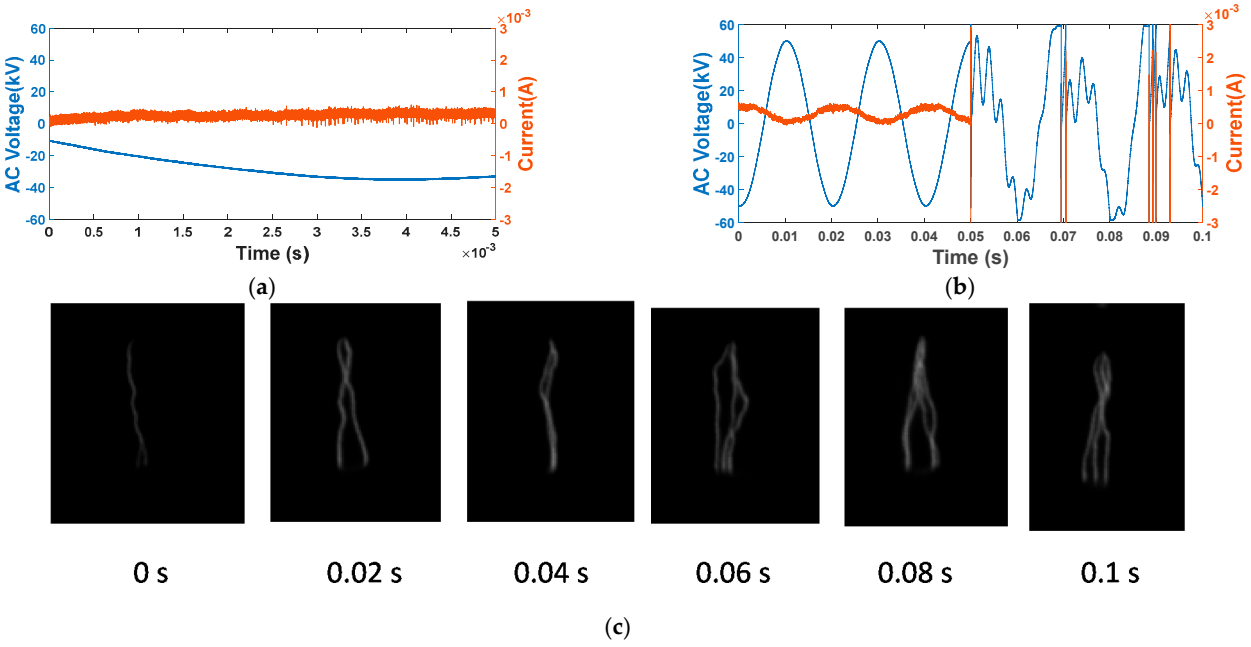

Figure 11. Voltage–current waveform for measuring partial discharge and breakdown voltages in 12.77% O_2–87.23% CO_2 (P = 8.8 bar abs, d = 10 mm): (**a**) negative partial discharge (PD), (**b**) breakdown on the positive cycle and (**c**) associated gaseous discharge with an expanding plasma channel as a function of time.

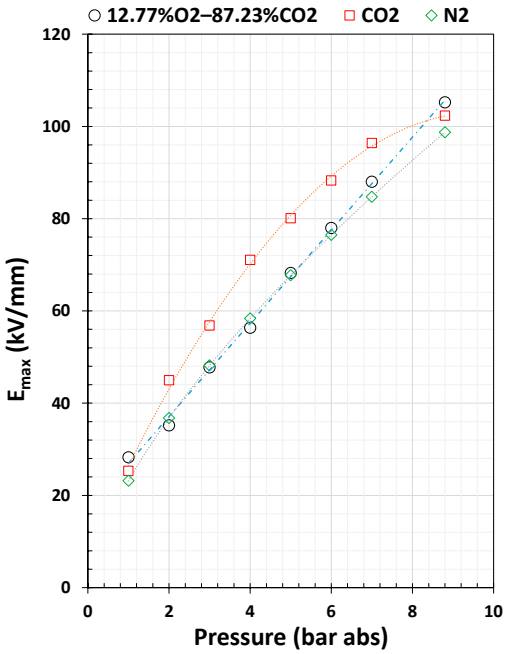

Figure 12. Negative-inception electric field in the visible +ultraviolet light as a function of gas pressure,12.77% O_2–87.23% CO_2 vs. CO_2 vs. N_2 (d = 10 mm, G_I = 60% is the relative luminous gain of the image recording system).

3.2. C_4F_7N Gas Based

C_4F_7N or Novec^{TM} 4710 was combined with a simple dilution natural gas/gas mixture (CO_2, O_2 and/or N_2). For quasi-homogeneous and divergent electric field distributions, the dielectric strength of the 20% C_4F_7N/80% CO_2 mixture was equivalent to that of pure SF_6 at equivalent pressure [7,8]. In practical applications, a reduction in the concentration of C_4F_7N was required to enable an increase in the filling pressure of the apparatus without liquefaction. Figure 13 summarizes the measured negative and the positive-inception and AC breakdown voltages for 20% C_4F_7N–80% CO_2 at various pressures up to 5 bar abs. The negative-inception voltage increased linearly with the increase of gas pressure. The breakdown characteristic of 20% C_4F_7N–80% CO_2 showed a nonlinear behavior over the gas pressure levels. The breakdown occurred under a negative AC voltage peak for pressure below 1.6 bar abs and on a positive AC voltage peak. The polarity reversal (PR) cross point at 1.6 bar abs corresponded to a positive-inception electric field of 84 kV/mm, calculated according to Equation (1). Below PR, negative and positive PDs were detectable until breakdown occurs. An example of negative and positive partial discharge voltage–current characteristics and its emission image (UV vs. UV + VIS) at 1.3 bar abs are shown in Figure 14.

Negative PDIV detection was possible via current measurement (current transformer 5-1) and via emission image. For high pressure (5 bar abs), multiple pulses around the positive cycle peak were detectable before the breakdown (see Figure 15). While negative partial discharge amplitude decreases with pressure increases, the intensity of positive partial discharge current increases. Increasing the applied voltage level induced denser current activity and consequently increased light emission (see Figures 14a and 15a); in turn, this generated a sufficient critical space charge avalanche to create a discharge. The positive glow streamer mode was identified as the breakdown mechanism for compressed 20% C_4F_7N–80% CO_2. The findings agreed with previous investigations on a 4% C_4F_7N–96% CO_2 gas mixture [6]. The streamer criterion was proven to fit the breakdown values for different electric field distributions [16]. The critical space charge size was given by the natural logarithm of the number of electrons $N_{critical}$ in the critical avalanche; Table 3 summarizes Ln ($N_{critical}$) for different C_4F_7N based gas mixtures. Increasing C_4F_7N content

led to an increase in the breakdown critical space charge and a larger gap between positive PDIV and breakdown, leading to a higher rate of gas molecules decomposition.

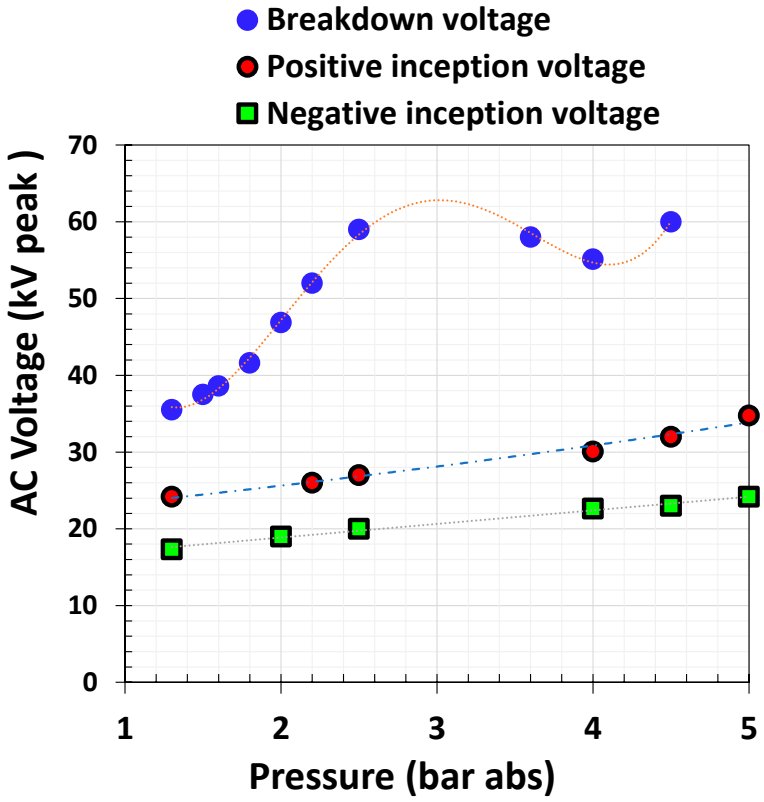

Figure 13. V_{mean} breakdown, positive and negative-inception voltages as a function of gas pressure (20% C_4F_7N–80% CO_2, d = 5 mm).

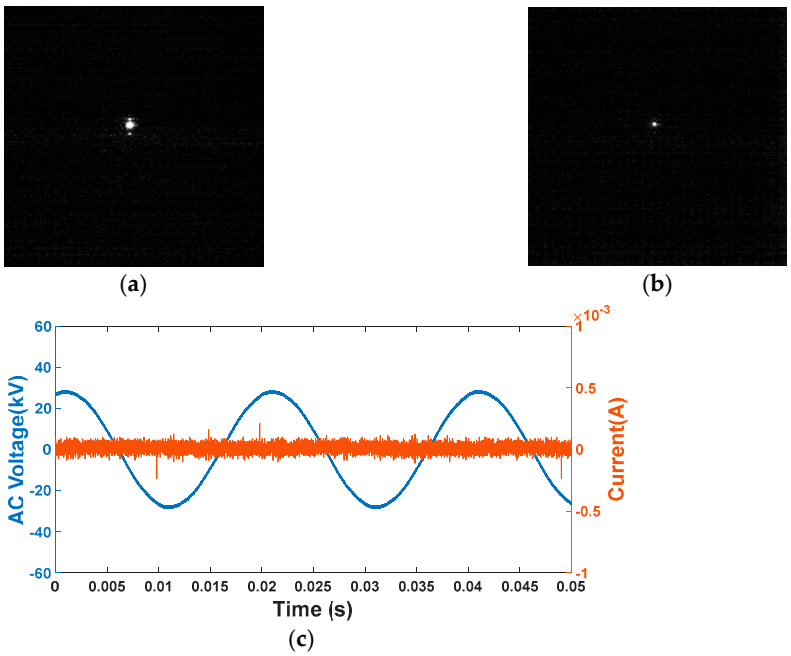

Figure 14. Positive-inception voltage in 20% C_4F_7N–20% CO_2: d = 5 mm, p = 1.3 bar abs, V = 30 kV, G_I = 60% is the relative luminous gain of the recording system in the: (**a**) visible + ultraviolet light (UV + VIS), (**b**) ultraviolet radiation and associated (UV) and (**c**) voltage–current waveform (Positive-inception voltage).

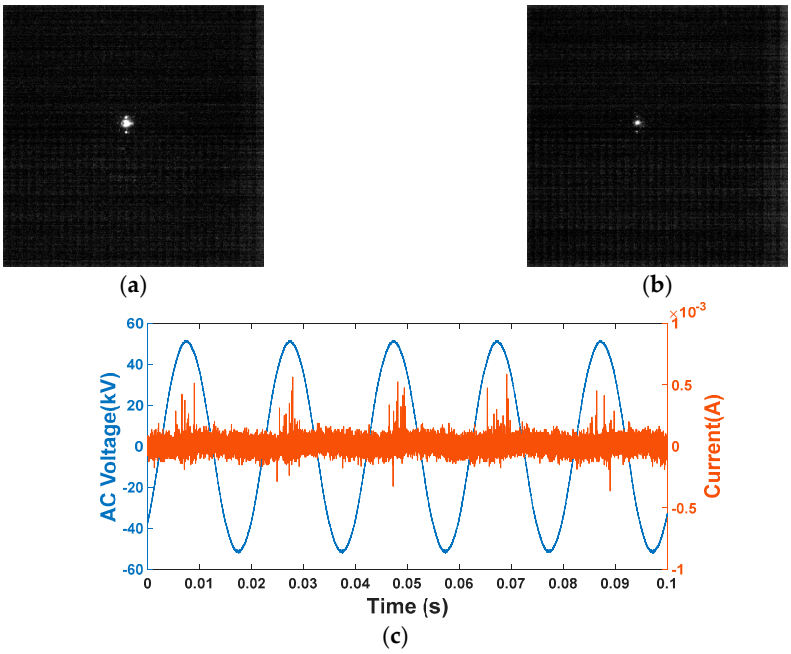

Figure 15. Positive-inception voltage in 20% C_4F_7N–20% CO_2: d = 5 mm, p = 5 bar abs, V = 52 kV, G_I = 60% is the relative luminous gain of the recording system in the (**a**) visible + ultraviolet light (UV + VIS), (**b**) ultraviolet radiation (UV) and (**c**) associated voltage–current waveform (PDs activity on positive half-cycle).

Table 3. Streamer criterion mechanism: critical breakdown space charge for different C_4F_7N based gas mixtures [17].

Gas/Gas Mixture	Ln ($N_{critical}$)
3.7% C_4F_7N–96.3% CO_2	6.228768
20% C_4F_7N–80% CO_2	8.448
C_4F_7N	14.56

To clarify the synergism between components of 20% C_4F_7N–80% CO_2 gas mixture, negative PDIV was identified for each pure component separately, i.e., C_4F_7N up to 1 bar abs (20% of the mixture), CO_2 up to 4 bar abs (80% of the mixture) and the final mixture of them up to 5 bar abs. The negative partial discharge inception electric field (PDIEF) E_{max} was calculated for each component according to Equation (1), reported to the final mixture pressure and plotted in Figure 16. For all the pressure ranges, PDIEF (C_4F_7N) was higher than PDIEF (20% C_4F_7N–80% CO_2), which in its turn was higher than PDIEF (CO_2). Synergism on PDIEF of 20% C_4F_7N–80% CO_2 gas mixture fits with the mean value of each individual component according to Equation (2). Based on PDIEF data of pure CO_2 (up to 8.8 bar abs, Figure 12) and pure C_4F_7N (up to 1 bar abs, Figure 15), three different variations with the increase of C_4F_7N content in a C_4F_7N–CO_2 gas mixture were identified. Table 4 summarizes the comparison between PDIEF (E_{max}) of CO_2 and C_4F_7N separately in C_4F_7N–CO_2 gas mixtures. At $9\pm^{1}_{0}$% C_4F_7N concentration, E_{max} (CO_2) = E_{max} (C_4F_7N). When C_4F_7N concentration < $9\pm^{1}_{0}$, Equation (2) was no longer applicable. Concerning polarity reversal, when the breakdown polarity changed from negative to positive half-cycle, the polarity reversal electric field E_{PR} was calculated according to Equation (1) for CO_2, SF_6, and different C_4F_7N–CO_2 gas mixtures and plotted in Figure 17. Fitting results show that E_{PR} (CO_2) = E_{PR} (9% C_4F_7N–91% CO_2) and E_{PR}(SF_6) = E_{PR} (22% C_4F_7N–78% CO_2). At the same time, the pressure of polarity reversal increased linearly with the increase of field utilization factor η. Increasing C_4F_7N content improved E_{PR} and polarity reversal pressure at the same time at a constant field utilization factor η (see Table 5). This variation was governed by a constant E_{PR} intrinsic characteristic for each gas/gas mixture.

$$E_{max}(20\%\ C_4F_7N - 80\%\ CO_2) = \frac{E_{max}(C_4F_7N - \text{Partial pressure}) + E_{max}(CO_2 - \text{Partial pressure})}{2} \quad (2)$$

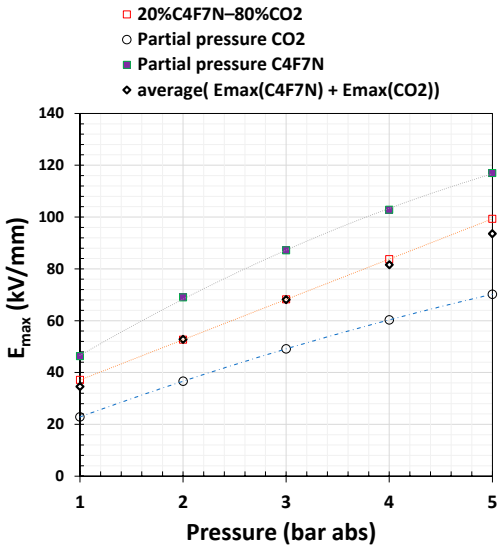

Figure 16. Synergistic effect on negative partial discharge inception electric field (PDIEF) as a function of gas pressure (20% C_4F_7N–80% CO_2 vs. partial pressure (CO_2) vs. partial pressure (C_4F_7N), d = 10 mm).

Table 4. Negative partial discharge inception electric field (PDIEF) (E_{max}) comparison between CO_2 and C_4F_7N as a function of component concentration.

Case	C_4F_7N/CO_2 Gas Mixture	
	% C_4F_7N	% CO_2
E_{max} (CO_2) > E_{max} (C_4F_7N)	<9 $\pm^1_0$	>91 $\pm^0_1$
E_{max} (CO_2) = E_{max} (C_4F_7N)	9 $\pm^1_0$	91 $\pm^0_1$
E_{max} (CO_2) < E_{max} (C_4F_7N)	>9 $\pm^1_0$	<91 $\pm^0_1$

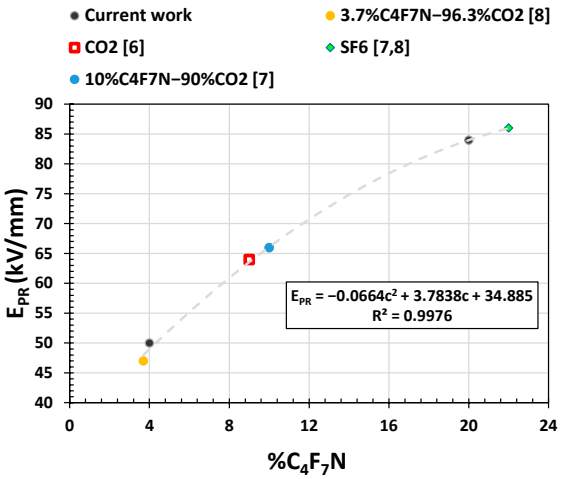

Figure 17. Synergistic effect on polarity reversal electric field of C_4F_7N–CO_2 gas mixtures compared to pure CO_2 and SF_6.

Table 5. Polarity reversal electric field E_{PR} according to Equation (1) (current work).

Gas/Gas Mixture	E_{PR} (kV/mm)	Pressure (bar abs)	η
20% C_4F_7N–80% CO_2	84	1.6	0.0385
4% C_4F_7N–96% CO_2	50	0.7	0.0385

3.3. $C_5F_{10}O$ Gas Based

The vaporization of $C_5F_{10}O$ or Novec ^{TM} 5110 was obtained above 26.9 °C. $C_5F_{10}O$ could only be used as an additive at a pressure below the saturated vapor pressure and could not be used in a pure state for insulation applications where the minimum operating temperature of an HV apparatus may drop to −25 °C or below. A mixture with a low concentration of a $C_5F_{10}O$ (4–6%) and a buffer gas ($O_2/N_2/CO_2$) resulted in an improvement of the dielectric strength [9].

Figure 18 reports AC breakdown measurements for 12.77% O_2–87.23% CO_2, 6% $C_5F_{10}O$–12% O_2–82% CO_2, and 20% C_4F_7N–80% CO_2 at various pressures and for a gap distance of 5 mm. All the gas mixtures show nonlinear behavior as a function of pressure and with different peak values. At 8.8 bar abs, the breakdown voltage of 6% $C_5F_{10}O$–12% O_2–82% CO_2 was equal to that of 12.77% O_2–87.23% CO_2. A saturation trend of the breakdown voltage was observed for 12.77% O_2–87.23% CO_2 and 6% $C_5F_{10}O$–12% O_2–82% CO_2 above 8.8 bar abs, while the increase for 20% C_4F_7N–80% CO_2 was linear. At 5 bar abs, the breakdown voltage of 20% C_4F_7N–80% CO_2 was 2 times higher compared to that of 6% $C_5F_{10}O$–12% O_2–82% CO_2 at 8.8 bar abs.

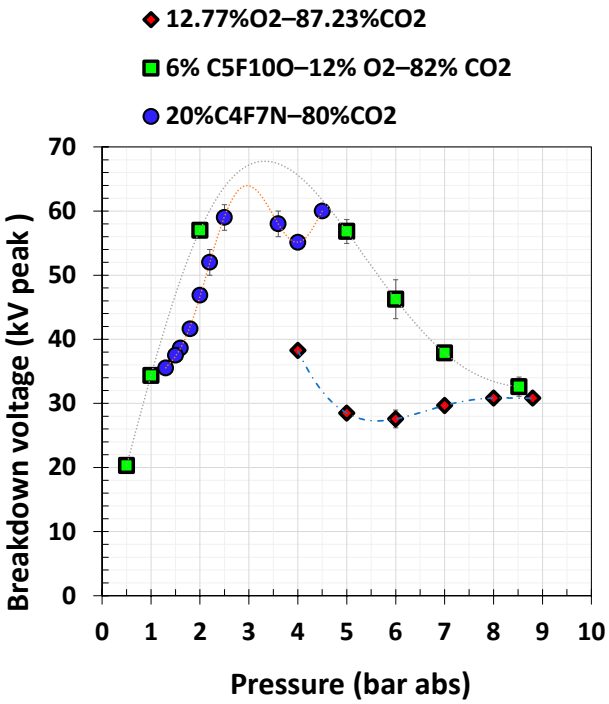

Figure 18. V_{mean} breakdown voltage as a function of gas pressure (12.77% O_2–87.23% CO_2 vs. 6% $C_5F_{10}O$–12% O_2–82% CO_2 vs. 20% C_4F_7N–80% CO_2, d = 5 mm).

The breakdown occurred under a negative AC voltage peak for pressures below 0.5 bar abs and on a positive AC voltage peak. The polarity reversal (PR) cross point at 0.5 bar abs corresponds to a positive-inception electric field of 36 kV/mm, calculated according to Equation (1). In terms of partial discharge activity, the 6% $C_5F_{10}O$–12% O_2–82% CO_2 exhibited a similar behavior compared with that of 12.77% O_2–87.23% CO_2 or 20% C_4F_7N–80% CO_2. Unlike 12.77% O_2–87.23% CO_2 and below PR, negative and positive PDs were detectable up to breakdown for the 6% $C_5F_{10}O$–12% O_2–82% CO_2. To explain the

latter behavior, pure $C_5F_{10}O$ at 0.54 bar abs, which corresponds to a 6% molar fraction of 9 bar abs total pressure, was evaluated separately, and the results are shown in Figure 19. High amplitude and positive polarity current pulses were detected during the positive cycle (see Figure 19a) before breakdown on the negative cycle (see Figure 19b), and a positive-inception electric field of 60 kV/mm was calculated according to Equation (1). On the other hand, C_4F_7N at 0.352 bar abs, which corresponds to a 4% molar fraction of 8.8 bar abs total pressure, exhibits similar behavior to $C_5F_{10}O$ with less dense positive polarity discharge activity (see Figure 19c). The corresponding positive-inception electric field was 70 kV/mm calculated according to Equation (1). The breakdown voltage of the $C_5F_{10}O$ (0.54 bar abs) was 1.09 times of C_4F_7N at 0.352 bar abs.

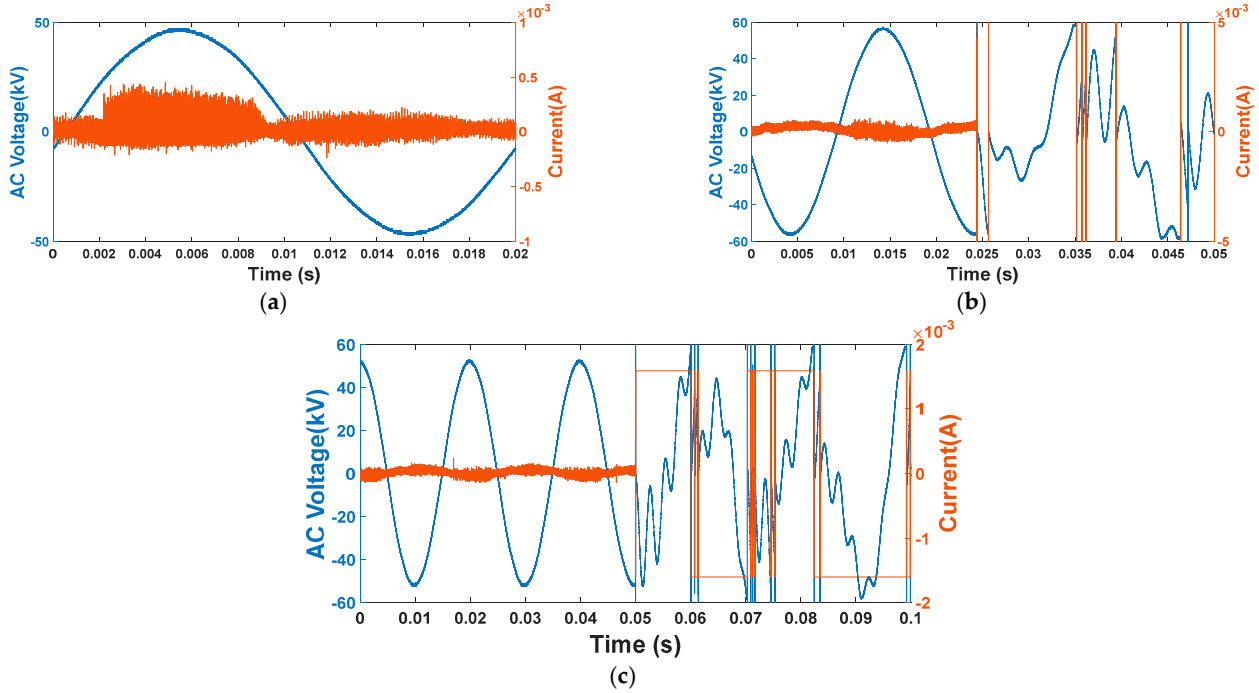

Figure 19. Voltage–current waveform for measuring partial discharge, and breakdown voltages ($C_5F_{10}O$ vs. C_4F_7N, gap distance d = 10 mm): (**a**) partial discharge ($C_5F_{10}O$, p = 0.54 bar abs), (**b**) breakdown on a negative cycle ($C_5F_{10}O$, p = 0.54 bar abs, V_b = 57.75 kV peak) and (**c**) breakdown on a negative cycle (C_4F_7N, p = 0.352 bar abs, V_b = 53 kV peak.

Above PR, the intensity of negative partial discharge current decreased with the increase of pressure. For high pressure (7 bar abs, see Figure 20), negative PDIV detection was not possible via current measurement (current transformer 5-1); however, the detection was performed via emission image. Before breakdown at high pressure (p = 6 bar abs), positive partial discharge appears in multiple pulsed within the positive AC half-cycle (see Figures 21a and 22). Increasing the applied voltage levels induced more current activity and a brighter emission image. The breakdown on the positive cycle was led by a positive-streamer sufficient space charge. 6% The 6% $C_5F_{10}O$–12% O_2–82% CO_2 presents denser positive partial discharge activities before the breakdown compared to the 4% C_4F_7N–96% CO_2 [6].

Negative partial discharge inception electric field (PDIEF) E_{max} was calculated according to Equation (1) for pure $C_5F_{10}O$ and C_4F_7N at sub-atmospheric pressures corresponding to the operational molar fraction without liquefaction in real indoor/outdoor high voltage applications and the results are shown in Figure 23. For this pressure range, PDIEF(C_4F_7N) was higher than PDIEF($C_5F_{10}O$) and, at 0.6 bar abs, PDIEF(C_4F_7N) was 2.18 times higher than PDIEF($C_5F_{10}O$). Figure 24 shows (PDIEF) E_{max} for 4% C_4F_7N–96% CO_2, 6% $C_5F_{10}O$–12% O_2–82% CO_2, and 20% C_4F_7N–80% CO_2 as a function of pressure. For all the gas mixtures, PDIEF was linear as a function of pressure, and PDIEF (6% $C_5F_{10}O$–12% O_2–

82% CO_2) was higher than PDIEF (4% C_4F_7N–96% CO_2). Above 3 bar abs, PDIEF (20% C_4F_7N–80% CO_2) > PDIEF (4% C_4F_7N–96% CO_2 and 6% $C_5F_{10}O$–12% O_2–82% CO_2).

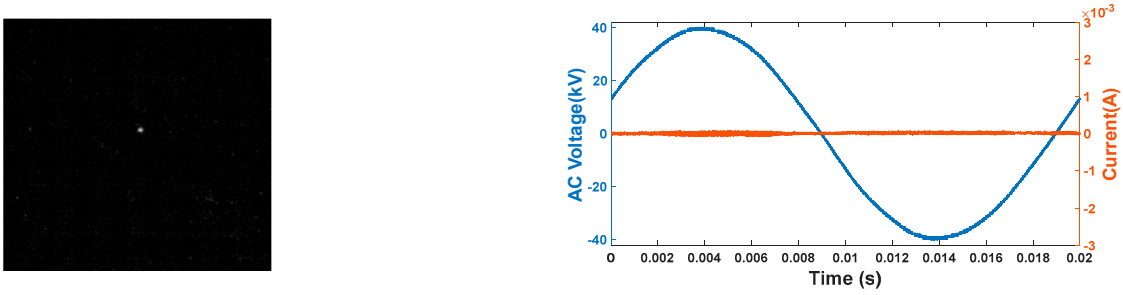

(**a**) (**b**)

Figure 20. Negative inception voltage in 6% $C_5F_{10}O$–12% O_2–82% CO_2: d = 10 mm, p = 7 bar abs, V = 40 kV, G_I = 60% is the relative luminous gain of the recording system in the: (**a**) visible + ultraviolet light (VIS + UV) and (**b**) associated voltage–current waveform (inception voltage).

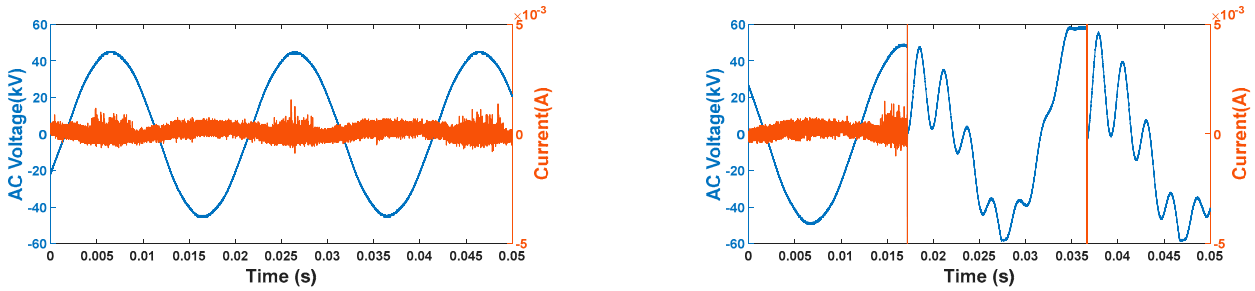

(**a**) (**b**)

Figure 21. Voltage–current waveform for measuring partial discharge, and breakdown voltages (6% $C_5F_{10}O$–12% O_2–82% CO_2, P = 6 bar abs, gap distance d = 5 mm): (**a**) partial discharge and (**b**) breakdown on a positive cycle.

(**a**) (**b**)

Figure 22. Partial discharge in 6% $C_5F_{10}O$–12% O_2–82% CO_2: d = 5 mm, p = 6 bar abs, V = 45 kV, G_I = 60% is the relative luminous gain of the recording system in the: (**a**) visible +ultraviolet light (VIS + UV) and (**b**) ultraviolet (UV) radiation along the electromagnetic spectrum.

To study the synergism between components of 6% $C_5F_{10}O$–12% O_2–82% CO_2 gas mixture, negative PDIV was identified for each pure component separately, i.e., $C_5F_{10}O$ up to 0.6 bar abs (6% of the mixture), 12.77% O_2–87.23% CO_2 up to 9.4 bar abs (94% of the mixture), and the final mixed gas up to 10 bar abs. The negative partial discharge inception electric field (PDIEF) E_{max} was calculated for each component according to Equation (1), reported to the final mixture pressure and plotted in Figure 25. For all the pressure ranges, PDIEF (6% $C_5F_{10}O$–12% O_2–82% CO_2) was higher than PDIEF (12.77% O_2–87.23% CO_2), which, in its turn, was higher than PDIEF ($C_5F_{10}O$). Synergism on PDIEF of 6% $C_5F_{10}O$–12% O_2–82% CO_2 gas mixture fits with the sum of each negative partial discharge inception electric field E_{max} individually component according to Equation (3).

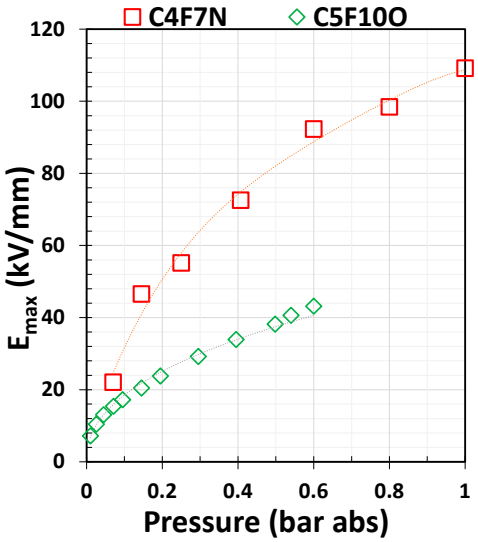

Figure 23. Negative-inception electric field as a function of gas pressure ($C_5F_{10}O$ vs. C_4F_7N, d = 10 mm).

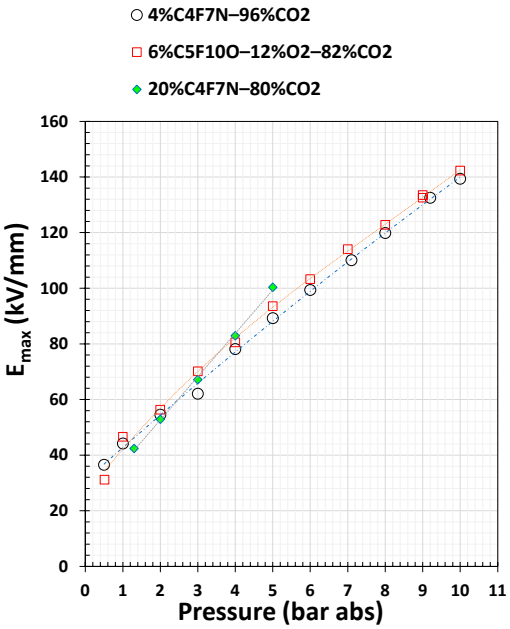

Figure 24. Negative-inception electric field as a function of gas pressure (6% $C_5F_{10}O$–12% O_2–82% CO_2 vs. 4% C_4F_7N–96% CO_2 vs. 20% C_4F_7N–80% CO_2, d = 10 mm).

Based on PDIEF data of pure 12.77% O_2–87.23% CO_2 (up to 9.4 bar abs) and pure $C_5F_{10}O$ (up to 0.6 bar abs), three different variations with the increase of $C_5F_{10}O$ content in a $C_5F_{10}O$–(12.77% O_2–87.23% CO_2) gas mixture were identified. Table 6 summarizes the comparison between PDIEF (E_{max}) of 12.77% O_2–87.23% CO_2 and $C_5F_{10}O$ separately in $C_5F_{10}O$–(12.77% O_2–87.23% CO_2) gas mixtures. At $19\pm^{1}_{0}$ $C_5F_{10}O$ concentration, E_{max} (12.77% O_2–87.23% CO_2) = E_{max}($C_5F_{10}O$).

Regarding polarity reversal, when the breakdown polarity changes from negative to positive cycle, the polarity reversal electric field E_{PR} was calculated according to Equation (1) for CO_2, 12.77% O_2–87.23% CO_2, and 6% $C_5F_{10}O$–12% O_2–82% CO_2 gas mixtures (see Table 7). At a constant field utilization factor η, decreasing the concentration of CO_2 reduces final E_{PR} and polarity reversal pressure. A linear trend was observed between polarity reversal pressure and final polarity reversal electric field E_{PR}. Comparing data in Tables 5

and 7, it could be observed that E_{PR} (4% C_4F_7N–96% CO_2) = E_{PR} (12.77% O_2–87.23% CO_2) and E_{PR} (6% $C_5F_{10}O$–12% O_2–82% CO_2) was less than E_{PR} (4% C_4F_7N–96% CO_2).

$$E_{max}(6\%C_5F_{10}O - 12\%O_2 - 82\%CO_2) = E_{max}(C_5F_{10}O - \text{Partial pressure}) + E_{max}(12.77\%O_2 - 87.23\%CO_2 - \text{Partial pressure}) \quad (3)$$

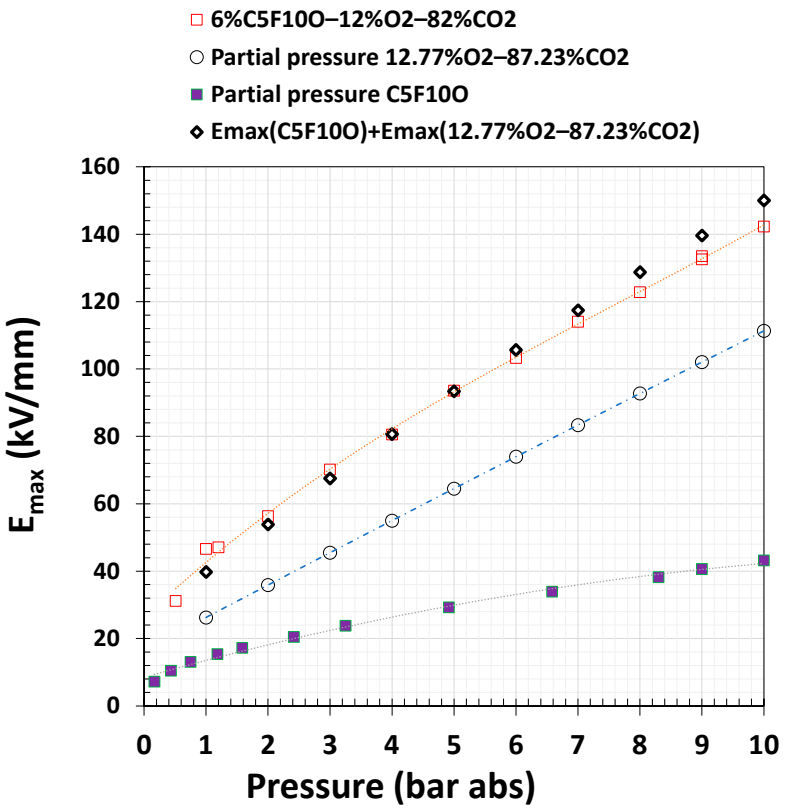

Figure 25. Synergistic effect on negative partial discharge inception electric field (PDIEF) as a function of gas pressure (6% $C_5F_{10}O$–12% O_2–82% CO_2 vs. partial pressure (12.77% O_2–87.23% CO_2) vs. partial pressure ($C_5F_{10}O$), d = 10 mm).

Table 6. PDIEF (E_{max}) comparison between 12.77% O_2–87.23% CO_2 and $C_5F_{10}O$ as a function of component concentration.

Case	$C_5F_{10}O$/12.77% O_2–87.23% CO_2 Gas Mixture	
	% $C_5F_{10}O$	%(12.77% O_2–87.23% CO_2)
E_{max} (12.77% O_2–87.23% CO_2) > E_{max} ($C_5F_{10}O$)	<19 $\pm_0^1$	>81 $\pm_1^0$
E_{max} (12.77% O_2–87.23% CO_2) = E_{max} ($C_5F_{10}O$)	19 $\pm_0^1$	81 $\pm_1^0$
E_{max} (12.77% O_2–87.23% CO_2) < E_{max} ($C_5F_{10}O$)	>19 $\pm_0^1$	<81 $\pm_1^0$

Table 7. Polarity reversal electric field E_{PR} according to Equation (1) for different gas mixtures-based CO_2.

Gas/Gas Mixture	E_{PR} (kV/mm)	Pressure (bar abs)	η
CO_2	64	2.5	0.0385
12.77% O_2–87.23% CO_2	50	1.6	0.0385
6% $C_5F_{10}O$–12% O_2–82% CO_2	36	0.5	0.0385

4. Discussion

Compared to CO_2, the addition of O_2 (12.77% O_2–87.23% CO_2) increased the critical reduced electric field strength from 82 Td to 90 Td (1 Td = 10^{-21} V.m^2) with ≈10% improvement [18,19]. N_2-O_2 gas mixtures exhibited better critical reduced electric field strength than CO_2–O_2 for oxygen content higher than 8% (see Figure 26). At 15 Td, the mixture 16% O_2–84% CO_2 exhibited the same value of reduced attachment Townsend coefficient as pure O_2 [18]. Compared to N_2 or N_2-O_2 gas mixtures, CO_2 or CO_2–O_2 mixtures had better arc-breaking capabilities. Oxygen was selected to be part of the gas mixture ($C_4F_7N/CO_2/O_2$) to reduce the generation rate of both carbon monoxide (main decomposition product) and fluorinated byproducts during arc quenching [20].

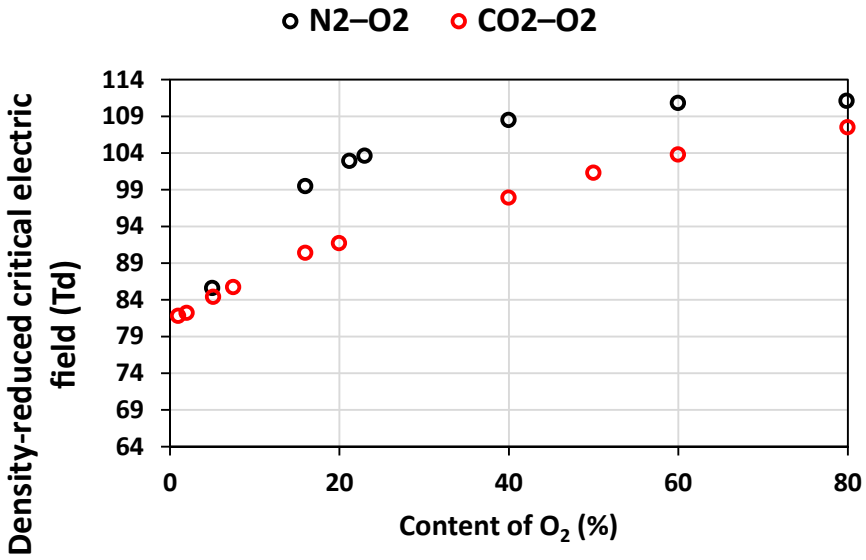

Figure 26. Density-reduced critical electric field of N_2–O_2 and CO_2–O_2 gas mixtures [19].

The analysis of the effective ionization coefficients in $C_5F_{10}O/O_2/CO_2$ [21,22] and C_4F_7N/CO_2 [23] gas mixtures showed a strong dependence of the effective ionization coefficient on the gas density. $C_5F_{10}O$ is characterized by an intrinsic dielectric strength highly dependent on the pressure, i.e., the increase of pressure increases the limiting dielectric strength. For a stationary value E/N of density reduced electric field (see Equation (4)), where:

- V: DC applied voltage;
- d: Insulation distance; and
- N: gas density, increasing the pressure decreases the applied voltage V, resulting in a decrease of the velocity and the energy of the emitted electrons.

The decrease of the energy of the swarm inhibits the generations in fractional negative ions result of dissociative attachment. The pure $C_5F_{10}O$ and C_4F_7N exhibit PDs activities on the AC positive half-cycle when the breakdown occurs on the negative half-cycle (see Figure 19b,c). The pure $C_5F_{10}O$ shows denser PDs activity than that of pure C_4F_7N. Moreover, for similar breakdown voltages, negative partial discharge inception electric field of C_4F_7N at 0.352 bar abs is 1.75 times higher than that of $C_5F_{10}O$ at 0.54 bar abs, as shown in Figure 23. The positive PDs incept by dissociative attachment of electrons in $C_5F_{10}O$ or C_4F_7N. Thynne and Harland [24] reported negative ions formed by low energy electron impact and attachment to C_4F_7N, using a Bendix time of flight spectrometer. Multiple dissociative attachment ions are formed (F^-, CN^-, CF_3^-, $C_2F_5^-$ and $C_3F_7^-$) in the range of appearance potential 0.3–12 eV. The appearance potential is defined as the energy required to produce the ion and its accompanying neutral fragment from a given molecule. The attachment cross-section of C_4F_7N is continuous and higher than SF_6 in the energy range

between 0.1 eV and 1 eV [25]. Hösl et al. [23] proved the existence of three types of anions (F^- or CN^- and/or $C_4F_7N^-$) at low energies and developed a model, including the anions electron detachment to fit their experimental breakdown data. Ranković et al. [26] detected and identified the C_4F_7N fragments (F^-, CN^-, $C_3F_4N^-$, $C_4F_6N^-$) by the electron energy loss spectroscopy and the dissociative electron attachment spectroscopy created at energies around ~1 eV.

The attachment cross-section $C_5F_{10}O$ [25] is similar to that of SF_6 for electron energies below 0.7 eV, and that it is substantially larger than that of SF_6 in the region between 0.7 eV and 10 eV. The formation of anions is governed by dissociative attachment to $C_5F_{10}O$. Dissociative electronic attachment leads to fragmentation of the $C_5F_{10}O$ molecules; different chemical species appear in the gas phase. The species generated in the gas phase cause a destabilization of the molecular texture and a weakening of the dielectric behavior of gas or gas mixture.

$$\frac{E}{N} = \frac{V}{Nd} \tag{4}$$

The SF_6 presents different behaviors of the electron attachment cross-section [27] in the incident energy of the electron E_i between 0 and 10 eVas shown in Figure 27. Electrons with low-energy < 0.6 eV and low-speed are generally absorbed by SF_6 molecules to form SF_6^- anion in a stable state. For unstable SF_6^- anions, the electrons auto-detaches after 68 ± 0.2 µs [28]. Dissociative attachment of electrons in SF_6 is dependent on the incident energy of the electrons E_i. For E_i between 0.6 eV and 2 eV, SF_5^- anions are produced by fragmentation of the parent SF_6 molecule. For E_i between 2 eV and 3.5 eV, no dissociative attachment occurs. For E_i between 3.5 eV and 10 eV, SF_4^-, SF_3^- and SF_2^- anions are produced. The previous dissociative attachment patterns in SF_6 result in multiple polarity reversal (at least 2) (+)/(−) and (−)/(+) as a function of the maximum electric field given by Equation (1) [7,8,14,29,30].

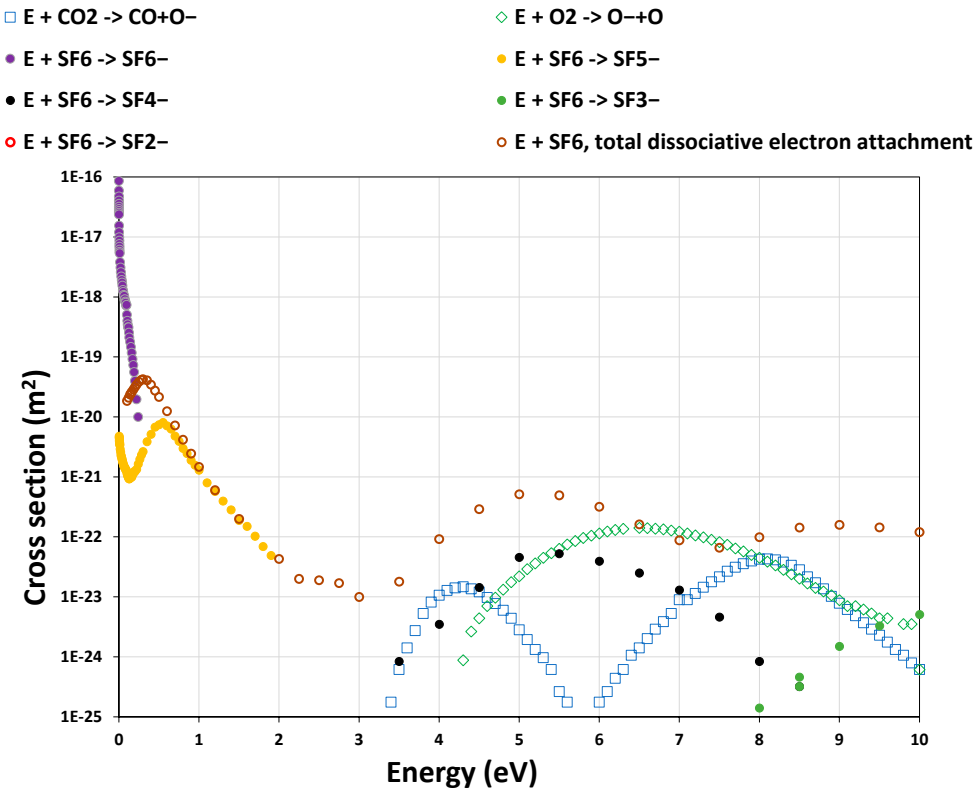

Figure 27. Dissociative attachment cross-section of SF_6 [27], CO_2 [31] and O_2 [32].

Only one polarity reversal happens in C_4F_7N/CO_2 mixtures and pure CO_2. The breakdown voltage in positive polarity becomes constraining and goes below the voltage in negative polarity when the pressure increases and/or the field tends to be divergent.

5. Conclusions

The breakdown characteristic as a function of pressure under non-uniform electric field distribution is linear for N_2 and strongly nonlinear for weak electronegative gas/gas mixture (CO_2, 12.77% O_2–87.23% CO_2) or strong electronegative gas/gas mixture (C_4F_7N, $C_5F_{10}O$, 4% C_4F_7N–96% CO2, 20% C_4F_7N–80% CO_2, 6% $C_5F_{10}O$–12% O_2–82% CO_2). The negative glow streamer mode is identified as the breakdown mechanism for compressed N_2.

For compressed 4% C_4F_7N–96% CO_2 and 6% $C_5F_{10}O$–12% O_2–82% CO_2 gas mixtures under non-uniform electric field distribution, the positive-streamer mode is identified as the breakdown mechanism. Breakdown and negative partial discharge inception voltages of 6% $C_5F_{10}O$–12% O_2–82% CO_2 are higher than those of 4% C_4F_7N–96% CO_2. For high pressure, negative PDIV detection is not possible via current measurement; the detection is feasible via emission image. At 8.8 bar abs, the breakdown voltage of 6% $C_5F_{10}O$–12% O_2–82% CO_2 is equal to that of 12.77% O_2–87.23% CO_2 (buffer gas). At 5 bar abs, the breakdown voltage of 20% C_4F_7N–80% CO_2 is 2 times higher compared with that of 6% $C_5F_{10}O$–12% O_2–82% CO_2 at 8.8 bar abs.

For 20% C_4F_7N–80% CO_2 gas mixture, synergism in negative partial discharge inception voltage/electric field fits with the mean value of each individual partial pressure component (C_4F_7N and CO_2). Based on partial discharge inception voltage/electric field data of pure CO_2 (up to 8.8 bar abs) and pure C_4F_7N (up to 1 bar abs), three different variations with the increase of C_4F_7N content in a C_4F_7N–CO_2 gas mixture was identified. At 9 $\pm^1_0$ C_4F_7N concentration, partial discharge inception electric field E_{max} (CO_2) = E_{max}(C_4F_7N). When C_4F_7N concentration < 9 $\pm^1_0$, the mean value of each partial pressure individual component (C_4F_7N and CO_2) is no longer applicable.

For 6% $C_5F_{10}O$–12% O_2–82% CO_2 gas mixture, synergism in negative partial discharge inception voltage/electric field (E_{max}) fits with the sum of each individual partial pressure component ($C_5F_{10}O$ and 12.77% O_2–87.23% CO_2). Based on partial discharge inception voltage/electric field data of 12.77% O_2–87.23% CO_2 (up to 9.4 bar abs) and pure $C_5F_{10}O$ (up to 0.6 bar abs), three different variations with the increase of $C_5F_{10}O$ content in a $C_5F_{10}O$–(12.77% O_2–87.23% CO_2) gas mixture was identified. At 19 $\pm^1_0$ $C_5F_{10}O$ concentration, E_{max} (12.77% O_2–87.23% CO_2) = E_{max}($C_5F_{10}O$).

Polarity reversal occurs under AC voltage when the breakdown polarity changes from negative to positive cycle. Polarity reversal electric field E_{PR} was quantified. Fitting results show that E_{PR} (CO_2) = E_{PR}(9% C_4F_7N–91% CO_2) and E_{PR}(SF_6) = E_{PR} (22% C_4F_7N–78% CO_2). The pressure of polarity reversal increases linearly with the increasing field utilization factor η. At a constant field utilization factor η, increasing C_4F_7N content improves E_{PR} and polarity reversal pressure. This variation is ruled by a constant E_{PR} intrinsic characteristic for each gas/gas mixture. The addition of O_2 in 12.77% O_2–87.23% CO_2 and $C_5F_{10}O$ in $C_5F_{10}O$–(12.77% O_2–87.23% CO_2) reduces final E_{PR} and polarity reversal pressure, E_{PR} (4% C_4F_7N–96% CO_2) = E_{PR} (12.77% O_2–87.23% CO_2) and E_{PR} (6% $C_5F_{10}O$–12% O_2–82% CO_2) < E_{PR} (4% C_4F_7N–96% CO_2) < E_{PR} (CO_2).

Author Contributions: Conceptualization, H.E.N., M.M., A.H. and G.W.; methodology, H.E.N.; validation, A.H.; formal analysis, H.E.N.; investigation, H.E.N.; writing—original draft preparation, H.E.N.; writing—review and editing, H.E.N., M.M., A.H. and G.W.; supervision, A.H.; project administration, A.H. and G.W.; funding acquisition, A.H. and G.W. All authors have read and agreed to the published version of the manuscript.

Funding: This research was funded by National Grid Electricity Transmission UK.

Institutional Review Board Statement: Not applicable.

Informed Consent Statement: Not applicable.

Data Availability Statement: Not applicable.

Conflicts of Interest: The authors declare no conflict of interest.

References

1. Niemeyer, L.; Pinnekamp, F. Leader Discharges in SF_6. *J. Phys. D Appl. Phys.* **1983**, *16*, 1031–1045. [CrossRef]
2. Mazurek, B.; Cross, J.D.; van Heeswijk, R.G. The effect of a metallic particle near a spacer on flashover phenomena in SF_6. *IEEE Trans. Electr. Insul.* **1993**, *28*, 219–229. [CrossRef]
3. Takahashi, T.; Yamada, T.; Hayakawa, N.; Yuasa, S.; Okabe, S.; Okubo, H. Corona stabilization effect in SF_6 gas viewed from sequential generation of partial discharge. In Proceedings of the 1999 Eleventh International Symposium on High Voltage Engineering, London, UK, 23–27 August 1999; Volume 3, pp. 88–91.
4. Piccin, R.; Mor, A.R.; Morshuis, P.; Girodet, A.; Smit, J. Partial discharge analysis of gas insulated systems at high voltage AC and DC. *IEEE Trans. Dielectr. Electr. Insul.* **2015**, *22*, 218–228. [CrossRef]
5. Ouss, E.; Beroual, A.; Girodet, A.; Ortiz, G.; Zavattoni, L.; Vu-Cong, T. Characterization of partial discharges from a protrusion in HVDC coaxial geometry. *IEEE Trans. Dielectr. Electr. Insul.* **2020**, *27*, 148–155. [CrossRef]
6. Nechmi, H.E.; Slama, M.E.A.; Haddad, A.M.; Wilson, G. AC Volume Breakdown and Surface Flashover of a 4% Novec^{TM} 4710/96% CO_2 Gas Mixture Compared to CO_2 in Highly Nonhomogeneous Fields. *Energies* **2020**, *13*, 1710. [CrossRef]
7. Nechmi, H.E.; Beroual, A.; Girodet, A.; Vinson, P. Fluoronitriles/CO_2 gas mixture as an eco-friendly alternative candidate to SF_6 in high voltage insulation systems. In Proceedings of the 2016 IEEE Conference on Electrical Insulation and Dielectric Phenomena (CEIDP), Toronto, ON, Canada, 16–19 October 2016; pp. 384–387. [CrossRef]
8. Nechmi, H.E.; Beroual, A.; Girodet, A.; Vinson, P. Fluoronitriles/CO_2 gas mixture as promising substitute to SF_6 for insulation in high voltage applications. *IEEE Trans. Dielectr. Electr. Insul.* **2016**, *23*, 2587–2593. [CrossRef]
9. Cigré Technical Brochure No 802, Working Group B3.45: Application of non-SF_6 Gases or Gas-Mixtures in Medium and High Voltage Gas-Insulated Switchgear. May 2020. Available online: https://e-cigre.org/publication/802-application-of-non-sf6-gases-or-gas-mixtures-in-medium-and-high-voltage-gas-insulated-switchgear (accessed on 5 January 2021).
10. Michelarakis, M.; Widger, P.; Beroual, A.; Haddad, A.M. Electrical Detection of Creeping Discharges over Insulator Surfaces in Atmospheric Gases under AC Voltage Application. *Energies* **2019**, *12*, 2970. [CrossRef]
11. Malik, N.H. Streamer Breakdown Criterion for Compressed Gases. *IEEE Trans. Dielectr. Electr. Insul.* **1981**, *EI-16*, 463–467. [CrossRef]
12. Saitoh, H.; Morita, K.; Kikkawa, T.; Kato, K.; Hayakawa, N.; Okubo, H. Impulse partial discharge and breakdown characteristics of rod-plane gaps in N_2/SF_6 gas mixtures. In Proceedings of the 2001 Annual Report Conference on Electrical Insulation and Dielectric Phenomena (Cat. No.01CH37225), Kitchener, ON, Canada, 14–17 October 2001; pp. 397–400. [CrossRef]
13. Saitoh, H.; Morita, K.; Kikkawa, T.; Hayakawa, N.; Okubo, H. Impulse partial discharge and breakdown characteristics of rod–plane gaps in air and N_2 gases. *Electr. Eng. Jpn.* **2004**, *148*, 36–43. [CrossRef]
14. Sadaoui, F.; Beroual, A. Influence of polarity on breakdown voltage of gases in divergent electric field under lightning impulse voltages. In Proceedings of the 2012 International Conference on High Voltage Engineering and Application, Shanghai, China, 17–20 September 2012; pp. 496–499. [CrossRef]
15. Sadaoui, F. Comparaison des Caractéristiques Electriques et Optiques des Décharges Glissantes sur Différents Types D'isolateurs dans le CO_2, le SF_6 et le N_2 et Leurs Mélanges à Différentes Pressions. Ph.D. Thesis, Ecole Centrale de Lyon, Université of Lyon, Lyon, France, 2013.
16. Hösl, A. Analysis of Electron Detachment in Pulsed Townsend Measurements. Ph.D. Thesis, ETH Zurich, Zürich, Switzerland, 2019. No. 26230.
17. Nechmi, H.E.; Beroual, A.; Girodet, A.; Vinson, P. Effective ionization coefficients and limiting field strength of fluoronitriles-CO_2 mixtures. *IEEE Trans. Dielectr. Electr. Insul.* **2017**, *24*, 886–892. [CrossRef]
18. Zhao, H.; Deng, Y.; Lin, H. Study of the synergistic effect in dielectric breakdown property of CO_2-O_2 mixtures. *AIP Adv.* **2017**, *7*, 095102. [CrossRef]
19. Haefliger, P.; Franck, C. Comparison of swarm and breakdown data in mixtures of nitrogen, carbon dioxide, argon and oxygen. *J. Phys. D Appl. Phys.* **2019**, *52*, 025204. [CrossRef]
20. Hermosillo, V.; Gregoire, C.; Vancell, D.; Ozil, J.; Kieffel, Y.; Pierres, E. *Performance Evaluation of CO_2/Fluoronitrile Mixture at High Short Circuit Current Level in GIS and Dead-Tank High-Voltage Circuit Breakers*; Paper A3-301; Cigré: Paris, France, 2018.
21. Egüz, E.; Chachereau, A.; Hösl, A.; Franck, C. Measurements of Swarm Parameters in C_4F_7N:O_2:CO_2, $C_5F_{10}O$:O_2:CO_2 and $C_5F_{10}O$:O_2:N_2 Mixtures. In Proceedings of the 19th International Symposium on High Voltage Engineering (ISH 2019), Budapest, Hungary, 26–30 August 2019.
22. Chachereau, A.; Franck, C.M. Electrical insulation properties of the perfluoroketone $C_5F_{10}O$. *J. Phys. D Appl. Phys.* **2018**, *51*, 335204. [CrossRef]
23. Hösl, A.; Chachereau, A.; Pachin, J.; Franck, C.M. Identification of the discharge kinetics in the perfluoronitrile C_4F_7N with swarm and breakdown experiments. *J. Phys. D Appl. Phys.* **2019**, *52*, 235201. [CrossRef]
24. Thynne, J.C.J.; Harland, P.W. Ionisation of pentafluoroethyl cyanide and heptafluoro-n-propyl cyanide by electron impact. *Int. J. Mass Spectrom. Ion Phys.* **1973**, *11*, 399–408. [CrossRef]

25. Chachereau, A. Electron and Ion Kinetics in Fluorinated Gases for Electrical Insulation. Ph.D. Thesis, ETH Zurich, Zürich, Switzerland, 2018. No. 25657.
26. Ranković, M.; Kumar, T.P.R.; Nag, P.; Kočišek, J.; Fedor, J. Temporary anions of the dielectric gas C_3F_7CN and their decay channels. *J. Chem. Phys.* **2020**, *152*, 244304.
27. Christophorou, L.G.; Olthoff, J.K. Electron interactions with SF_6. *J. Phys. Chem. Ref. Data* **2000**, *29*, 267. [CrossRef]
28. Harland, P.W.; Thynne, J.C.J. Autodetachment lifetimes, attachment cross sections, and negative ions formed by sulfur hexafluoride and sulfur tetrafluoride. *J. Phys. Chem.* **1971**, *75*, 3517. [CrossRef]
29. Guo, C.; Wang, T.; Li, Z.; Zhang, Q.; Wen, T.; You, H.; Qin, Y.; Ma, J.; Wang, H.; Li, Y. The reversal of SF_6/N_2 gas mixtures polarity effect under lightning impulse. In Proceedings of the 2015 IEEE 11th International Conference on the Properties and Applications of Dielectric Materials (ICPADM), Sydney, NSW, Australia, 19–22 July 2015; pp. 176–179. [CrossRef]
30. Bujotzek, M.; Seeger, M. Parameter dependence of gaseous insulation in SF_6. *IEEE Trans. Dielectr. Electr. Insul.* **2013**, *20*, 845–855. [CrossRef]
31. Itikawa, Y. Cross Sections for Electron Collisions with Carbon Dioxide. *J. Phys. Chem. Ref. Data* **2002**, *31*, 749. [CrossRef]
32. Itikawa, Y. Cross Sections for Electron Collisions with Oxygen Molecules. *J. Phys. Chem. Ref. Data* **2009**, *38*. [CrossRef]